

## PIV Measurements of the Pressure Driven Flow Inside a T-Shaped Microchannel Junction

Jayho Choi\* · In-Seop Lee†

### T형 마이크로채널 연결부 압력구동 유동의 PIV 계측

최제호\* · 이인섭†

**Abstract.** A custom micro-PIV optics assembly has been used to measure the flow field inside a T-junction of a microchannel. The micro-PIV system consists of microscope objectives of various magnifications, a dichroic cube, and an 8-bit CCD camera. Fluorescent particles of diameters 620 nm have been used with a Nd:YAG laser and color filters. A programmable syringe pump with Teflon tubings were used to inject particle-seeded distilled water into the channel at flow rates of 2.0, 4.0, 6.0 mL/hr. The microchannels are fabricated with PDMS with a silicon mold, then O<sub>2</sub>-ion bonded onto a slide glass. Results show differences in flow characteristics and resolution according to fluid injection rates, and magnifications, respectively. The results include PIV data with vector-to-vector distances of 2 μm with 32 pixel-square interrogation windows at 50% overlap.

**Key Words :** PIV, Microfluidics(마이크로유동), T-Shaped Junction(T형 연결부), Microchannel(마이크로채널), Pressure-Driven Microscale Flow(압력구동 미세유동)

### 1. Introduction

A lab-on-a-chip, the integration of various biochemical/biomedical analyses onto a single chip, consists of numerous microfluidic components such as valves, pumps, and channels of different geometry for various mixing, sorting, and dispersion processes involved. The fluid inside the whole channel system is generally pressure-driven, or electrokinetically-driven, and various literatures involving the physical phenomena inside microchannels have been published.<sup>(1,2)</sup>

Until recently, microfluidic researches were carried out with scalar pressure or temperature measurements or the calculation of pixel intensity distribution by the use of a CCD camera and uncaged fluorescent dye.<sup>(2,3)</sup> With the development of microfluidic devices in

various fields such as biomedicine and chemical analysis, the need for quantitative flow field measurement inside microchannels of various geometry are growing in interest. Although fluid flows in microchannels are of low Reynolds number and the general flow pattern predictable, the velocity field of the fluid inside the whole channel is difficult to measure. Also, many such channels are used for microscale analyses such as chemical mixing, particle/molecule sorting, and dispersion control, for which the specific flow characteristics are difficult to analyze quantitatively.<sup>(3)</sup> Flow visualization and quantitative analysis of flows in microchannels are necessary for the development of efficient active and passive mixers.

Particle image velocimetry (PIV), which has become an indispensable tool in fluid flow field measurements, have been successfully applied for flow measurements

\*LG Electronics, jayho@LGE.com

†Nanoptic Inc., islee@nanoptic.net

in microscale structures. Santiago *et al.*<sup>(4)</sup> measured the Hele-Shaw Flow around a microscale circular structure, at a vector resolution of  $3.2\ \mu\text{m} \times 3.2\ \mu\text{m}$ . Meinhart *et al.*<sup>(5,6)</sup> also applied PIV to measuring the flow inside a microfabricated inkjet printhead, and a straight microchannel at a resolution of  $5.0\ \mu\text{m} \times 1.3\ \mu\text{m}$ . Santiago *et al.* and Meinhart *et al.* both used intensified CCD cameras with a full upright epi-fluorescence microscope system.

In this paper, a relatively low-cost, home-assembled epi-fluorescence optic system was used for the measurement of the flow inside a T-shaped microchannel junction with a non-intensified 8-bit CCD camera, relatively low cost compared to any intensified CCD camera. An early version of this system was used to measure the flow field inside a straight microchannel by Lee *et al.*<sup>(7)</sup>, and with the addition of a micro-positioner, the flow field at multiple measurement planes were analyzed.<sup>(8)</sup> In this paper, the micro-PIV system was improved in terms of magnification factor and the resolution was doubled as a result. With further improvement with higher resolution CCD cameras (i.e. 4 mega-pixels) and multiple syringe pumps, this system will be used as a high-resolution analysis tool for further research in microscale mixers.

## 2. Method and Apparatus

### 2.1 Seeding Particles

Certain requirements must be met in order for particles to be used in micro-PIV: its size must be small enough to accurately follow the flow, but large enough to be imaged through the optics and onto the CCD cell. Red fluorescent particles of 620 nm in diameter were used, having excitation and emission wavelengths of 530 nm and 612 nm, respectively.

Also, the Brownian motion of the particles is in effect and its error must be taken into account. According to Santiago *et al.*<sup>(4)</sup> the relative error

of the velocity gradient due to the Brownian motion can be estimated by:

$$\varepsilon_B = \frac{1}{u\lambda} \sqrt{\frac{2D}{\Delta t}} \quad (1)$$

where  $D$  is the diffusion coefficient, and  $\Delta t$  the time interval.

Taking into account the diffusive uncertainty, which is proportional to  $\varepsilon_B/\sqrt{N}$ <sup>(4)</sup>, for this experiment  $u \sim 37\ \text{mm/s}$  and  $\Delta t \sim 5\ \mu\text{s}$ , and 100 instantaneous velocity vector fields were ensemble-averaged to obtain the mean velocity field, the error due to Brownian motion can be approximated to be less than 1%. Particle density in the working fluid was set to 0.1% by volume.

### 2.2 Microchannel

The 3D draft and the specifications of the T-junction in the microchannel used in the experiment are shown in Fig. 1. The depth of the channel is  $50\ \mu\text{m}$ , with the main straight channel width of  $300\ \mu\text{m}$ , and  $5000\ \mu\text{m}$  in length. A  $50\ \mu\text{m}$  width

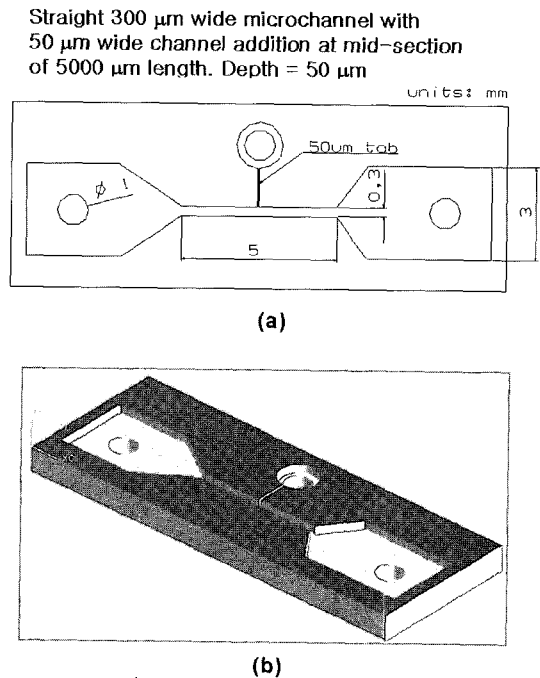


Fig. 1. Dimensions and geometry of the microchannel

channel exists perpendicular to the main straight channel at the mid section, forming a T-junction with a 300  $\mu\text{m}$  width for the horizontal channel and a 50  $\mu\text{m}$  width for the vertical channel. The channel was cast on PDMS from a silicon mold, which was then  $\text{O}_2$ -ion bonded onto a slideglass. The three circular holes that can be seen in Fig. 1 were bored on the PDMS for the insertion of Teflon tubings. Only the leftmost hole was used as the input for the flow, leaving the other two holes open at atmospheric pressure, each with an additional 100 mm long Teflon tubing attached at the end.

The channel can be firmly bolted in front of the microscope objective on a slot structure which is mounted on a 5 degree-of-freedom(DOF) micro-stage. The 5 DOF microstage is a home-made assembly of multiple translation stages, and provides rotation in all three directions, in addition to translations within the focal plane of the microscope

objective.

### 2.3 Imaging Optics

The schematic of the micro-PIV system optics is shown in Fig. 2 It consists of the microscope objective, a custom-made dichroic cube, the focusing tube, and a 8-bit 1 K $\times$ 1 K CCD camera.

Fig 2(a) shows an example on how the custom-made optics may be used for PIV measurement. The two microscope objectives used in this experiment were of magnifications 50 X and 100 X, with working distances of 13 mm, and 6 mm respectively. These infinity-corrected long working distance objectives are plano apochromats, with depths of focus of 0.9  $\mu\text{m}$  and 0.6  $\mu\text{m}$ , and resolving powers of 0.5  $\mu\text{m}$  and 0.4  $\mu\text{m}$  for the 50 X, 100 X magnifications. The measurement depth, according to Meinhart *et al.*<sup>(6)</sup>, can be calculated to be approximately 8  $\mu\text{m}$  and 6  $\mu\text{m}$  for the 50 X and

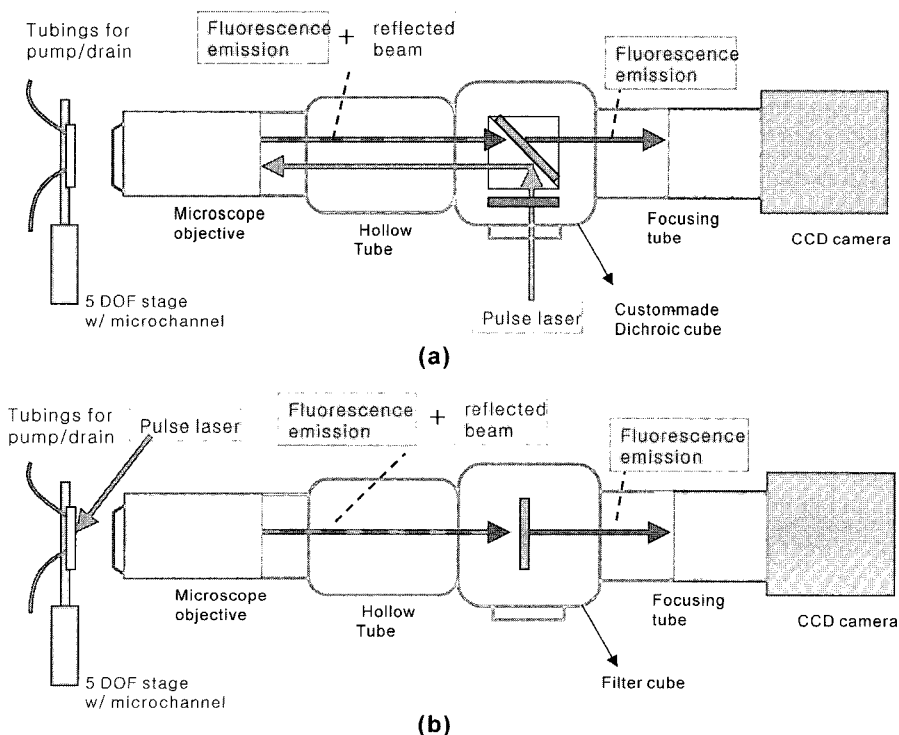


**Fig. 2.** Schematics of the custom-made Micro-PIV optics

(a) 50 X setup, used with 50 X objective, (b) 100 X setup, used with 100 X objective

100 X setup, respectively.

The microscope objective is attached to a hollow tube, which was mounted on a micro-stage, enabling precise movement along the z-axis, as seen in Fig. 2. The hollow tube is then connected to the dichroic cube via a sliding tube to isolate the beam path in darkness even when the hollow tube's horizontal position is adjusted. The dichroic cube is then connected to the focusing tube, which is a series of lenses used to focus the emission beams onto the CCD cell of the camera. The focusing tube is firmly attached to the CCD camera, and all optic components were setup on an optical rail for precise alignment of the beam path. The beam path shown in Fig. 2(a) is typical for epi-fluorescence microscopy, and this setup was used for measurements with the 50 X objective.

Fig 2(b) shows another optics setup, which was used for measurements with the 100 X objective, and enables maximum laser power for better illumination of the field of view without endangering the optics system to the high intensity of the laser beam.

The green pulse laser used is a two-head Nd:YAG laser with a maximum power output of over 300 mJ with a wavelength of 532 nm. The dichroic cube consists of three main optics components: the excitation filter, the dichroic mirror, and the emission filter, for which the characteristic wavelengths were custom-made to meet the 530 nm excitation and 612 nm emission wave-lengths of the fluorescent particles.

The CCD camera was synchronized with the pulse laser with the camera's shutter feedback as the master signal. Time delays of 3~5  $\mu$ s between particle images were needed for the flow.

### 3. Experimental Results

The microchannel was held in front of the microscope and its position adjusted with the micrometers attached to the microstage. Angular adjust-

ments of the microchannel were made by using the z-direction translation micrometer and angular positioning micrometers: part of the channel walls in contact with the glass slide were initially brought to focus, and by rotating the angular micrometers of the microstage with the z-direction micrometer of the hollow tube, a uniform focus along the x and y direction was confirmed, thus positioning the microchannel parallel to the object plane of the microscope objective.

The object plane was positioned at about the mid-depth of the channel, at approximately 25 mm from its bottom surface. This was done by focusing on the bottom and top surface walls of the channels, and moving the microscope objective in reference to those focused z-coordinates. Translation of the microscope objective was done by the micrometer attached to the hollow tube.

Distilled water was used as the working fluid, and a syringe pump was used with a 5 mL glass syringe at flow rates of 2.0, 4.0, and 6.0 mL/hr. The field of view(FOV) for the experiment is shown in Fig. 3: a rectangular area was selected which included the 50  $\mu$ m channel in the center. The FOV for the 50 X and 100 X setups were approximately 200  $\mu$ m  $\times$  200  $\mu$ m and 100  $\mu$ m  $\times$  100  $\mu$ m, respectively. With a 32-pixel square interrogation window at 50% overlap, this leads to a vector plot result with a vector-to-vector distance of approximately 4  $\mu$ m, and 2  $\mu$ m for the 50 X and 100 X setups, respectively.

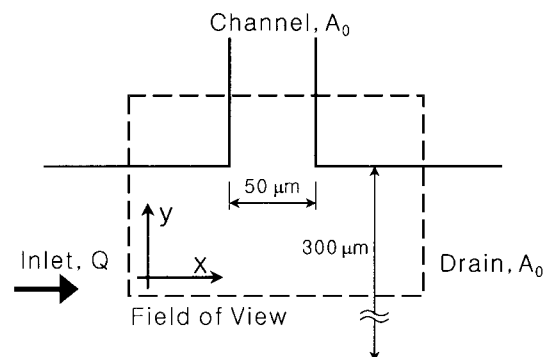


Fig. 3. Field of view of PIV measurements

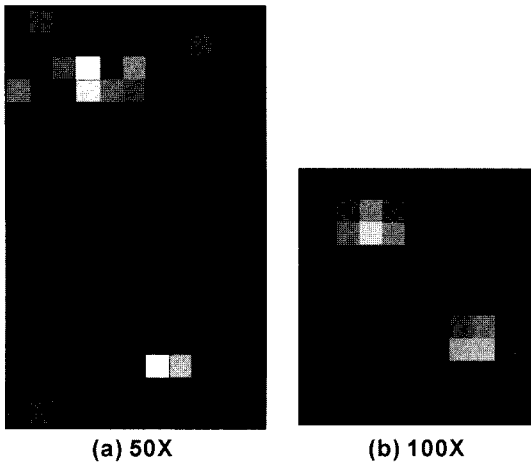


Fig. 4. Particle images with (a) 50 X and (b) 100 X setups.

Acquired raw particle images showed particle sizes of approximately 3~6 pixel-area and 7~10 pixel-area for the 50 X and 100 X setups, respectively, as shown in Fig. 4. Due to the small field of view, the particle images acquired with the 100 X setup were low in brightness relative to the increase in laser intensity. 100 instantaneous velocity vector fields were averaged to obtain each mean velocity vector fields, and are shown in Fig 5 through Fig 7

### 3.1 The 50 X Setup

Fig 5 shows the mean vorticity contour plots

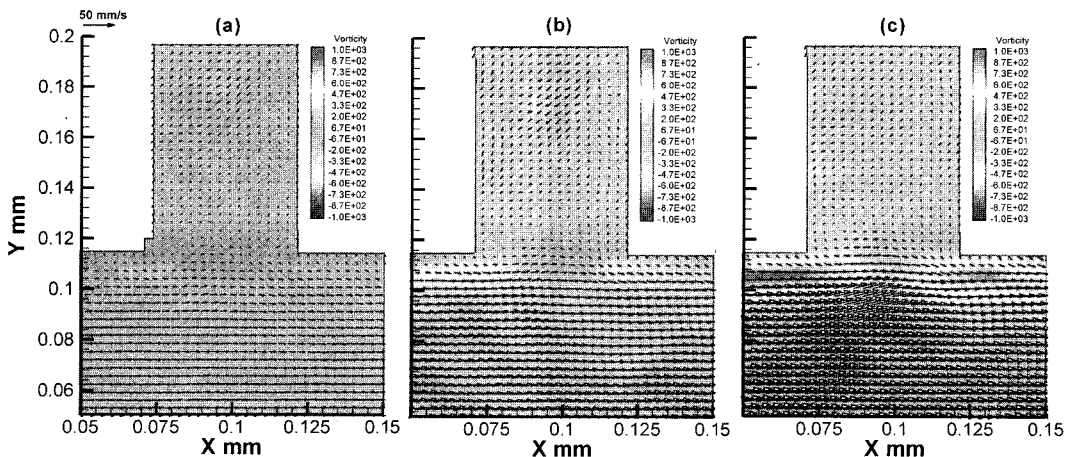


Fig. 5. Mean velocity vector field at the T-junction with 50 X setup, at flow rates of : (a) 2.0 mL/hr, (b) 4.0 mL/hr, (c) 6.0 mL/hr

and mean velocity vector field measured with the 50 X setup, plotted with the same reference vector magnitude. The flow direction is from left to right, with the x and y axis increments shown in millimeters. Fig. 5(a), 5(b), and 5(c) are the results for fluid injection rates of 2.0, 4.0 and 6.0 mL/hr, respectively. It is found that the main horizontal flow from left to right slightly deforms as it passes the 50  $\mu$ m channel and that the flow inside the 50  $\mu$ m channel is negligible for all fluid injection rates. However, the vorticity field along the wall of the 300  $\mu$ m-width main channel, is increased in strength as the fluid injection rate is increased. A discontinuity in the vorticity field is observed at the entrance of the 50  $\mu$ m channel, due to the deformation of the velocity field in that region. It is noted that the maximum vorticity value is located slightly offset from the wall surface. This is assumed to be due to the erroneous vector measurements at the wall surface.

### 3.2 The 100 X Setup

The mean velocity vector field measured with the 100 X setup is shown in Fig. 6, plotted with the same reference vector magnitude. The entrance region of the 50  $\mu$ m channel is plotted to better visualize the

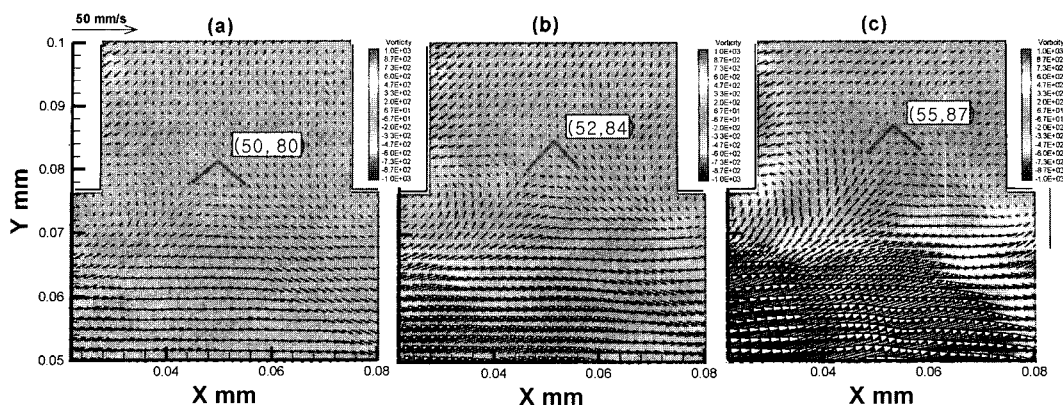


Fig. 6. Mean velocity vector field at the T-junction with 100 X setup, at flow rates of: (a) 2.0 mL/hr, (b) 4.0 mL/hr, (c) 6.0 mL/hr

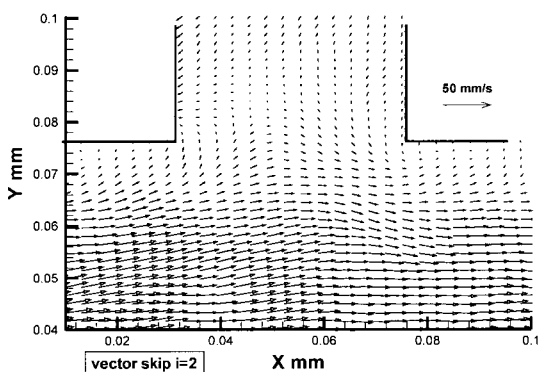


Fig. 7. Mean velocity vector field result at the T-junction with 100 X setup, at flow rate 4.0 mL/hr (only every 3rd vector in the x-direction is plotted)

difference between Fig. 6(a) through Fig. 6(c). Figure 6(a), 6(b), and 6(c) are the results for fluid injection rates of 2.0, 4.0, and 6.0 mL/hr, respectively. Compared with the results in Fig. 5, the resolution has been doubled, and a vector-to-vector distance of approximately  $2\ \mu\text{m}$  can be observed. Also, a difference in the amount deformation of the main horizontal flow is found: the distance at which the flow entering the  $50\ \mu\text{m}$  channel increasing with the fluid injection rate. The coordinates of the maximum entry distances of the particles into the  $50\ \mu\text{m}$  channel are estimated to be (50, 80), (52, 84), and (55, 87). The positions are marked in Fig 6 with a red bracket, the corner of the bracket indicating the coordinates.

Fig 7 shows a full-field-of-view mean velocity

vector field with a fluid injection rate of 4.0 mL/hr, measured with the 100 X setup. Only every 3<sup>rd</sup> vector in the x-direction is plotted. The erroneous velocity gradient in the y-direction near the left edge of the vector field is assumed to be due to particles attached to the wall surface, or over-sized, accumulated particle chunks that cause erroneous vector results in its vicinity.

#### 4. Conclusion

A custom-made epi-fluorescence micro-PIV optics setup was used to measure the velocity field in the T-shaped junction of a microchannel. A mean velocity vector field of vector-to-vector distances of  $2\ \mu\text{m}$  was obtained with a 100 X magnification setup, used with a non-intensified CCD camera and a 300 mJ pulse laser. Results showed the deformation of the main flow stream in the  $300\ \mu\text{m}$  wide channel, when the flow passes the entrance region of a smaller  $50\ \mu\text{m}$  wide channel. The amount of deformation was found to increase as the fluid injection rate was increased.

The advantage of the current micro-PIV setup is its low cost : making use of a relatively low-cost CCD camera, and without the need of a full-set epi-fluorescence microscope.

This micro-PIV setup, improved with, higher-

resolution CCD cameras and various fluid injection devices, will be used for further studies in microscale fluid mixing.

## REFERENCES

- 1) Deshpande, M., Greiner, K.B., Gilbert, J.R., Bousse, L., Chow, A. and Kopf-Sill, A.R., 1999, "Analysis of Multicomponent Sample Transport in Electrokinetic Microchemical Systems," Tech. Proc. of the 10<sup>th</sup> Int. Conf. on Solid-State Sensors and Actuators", Sendai, Japan, June 7~10.
- 2) Molho, J.I., Herr, A.E., Kenny, T.W., Mungal, M. G., St. John, P.M., Garguilo, M.G., Paul, P.H., Deshpande, M. and Gilbert, J.R., 1998, "Fluid Transport Mechanisms in Microfluidic Devices," ASME International Mechanical Engineering Congress and Exposition, DSC-Vol.66.
- 3) Stroock, A.D., Dertinger, S.K.W., Ajdari, A., Mezic, I., Stone, H.A. and Whitesides, G.M., 2002, "Chaotic Mixer for Microchannels," *Science*, Vol.295, pp.647~651.
- 4) Santiago, J.G., Wereley, S.T., Meinhart, C.D., Beebe, D.J. and Adrian, R.J., 1998, "A Particle Image Velocimetry System for Microfluidics," *Exp. in Fluids*, Vol.25, pp.316~319.
- 5) Meinhart, C.D. and Zhang, H., 2000, "The Flow Structure Inside a Microfabricated Injet Printhead," *J. of Microelectromechanical Systems*, Vol.9(1), pp. 67~75.
- 6) Meinhart, C.D., Wereley, S.T. and Santiago, J.G., 1999 "PIV Measurements of a Microchannel Flow," *Exp. in Fluids*, Vol.27, pp.414~419.
- 7) Lee, I., Choi, J. and Lee, I.S., 2001, "PIV Measurements of a Microfluidic Element Fabricated in a Plastic Chip," *Proc. of the KSME 2001 Fall Annual Meeting B*, pp.400~404.(in Korean)
- 8) Lee, I.S. and Lee, I., 2002, "A Three-Dimensional Measurement of Microchannel Flow Using Micro-PIV," *J. of Visualization*, Vol.22(1), pp.21~24.